

Simulation of an RPC Off-Axis Detector

R. Ray

Detector Description

An RPC based detector has been proposed as an alternate to the baseline liquid scintillator design for the NOvA off-axis experiment. A detailed description of the RPC detector can be found in Appendix A of the NovA proposal [1]. An engineering note also exists [2]. The proposed RPC detector consists of 1200 identical 42-metric-ton modules. Each module is 8.534 m long, 2.438 m high and 2.6 m deep. The modules are stacked in an array of 75 planes where each plane is 2 modules wide and 8 modules high, as shown in Figure 1.

Each module consists of 13 vertical planes of particleboard absorber interleaved with double planes of RPCs. Two end plates (Figure 2) provide the mechanical rigidity of the module. The weight of the module is supported by two bottom angles that transfer the load to four corner posts. The corner posts, also shown in Figure 2, are composed of two 1.27 cm thick aluminum plates sandwiched around a 7.62 cm thick particleboard. The whole structure is reinforced by 10 ribs, each 0.3175 cm thick, welded to the endplates and angles.

There are 12 RPC detector units per module. A detector unit consists of 6 RPC chambers arranged 3 across and 2 deep. An RPC is comprised of two parallel sheets of 3 mm thick glass with a 2 mm gas volume. The glass plates are held apart with plastic spacers around the edge of the chamber as well as inside the active volume. The RPC package is sandwiched between two particleboards that carry readout strips and that also contribute to the absorber volume. The RPC detector units are separated by 15.24 cm of particleboard absorber. The first and last absorber planes in a module are half as thick as the others. Thus, when taken together with the first and last planes of the preceding and succeeding modules, they result in a uniform sampling thickness across module boundaries.

One of the design goals of the RPC detector was to minimize dead space between the active components. There is a 1.27 cm vertical gap and a 0.9525 cm horizontal gap between RPCs in adjacent modules. In addition, each RPC chamber has a 5 mm dead space around the outer edge due to the plastic spacers.

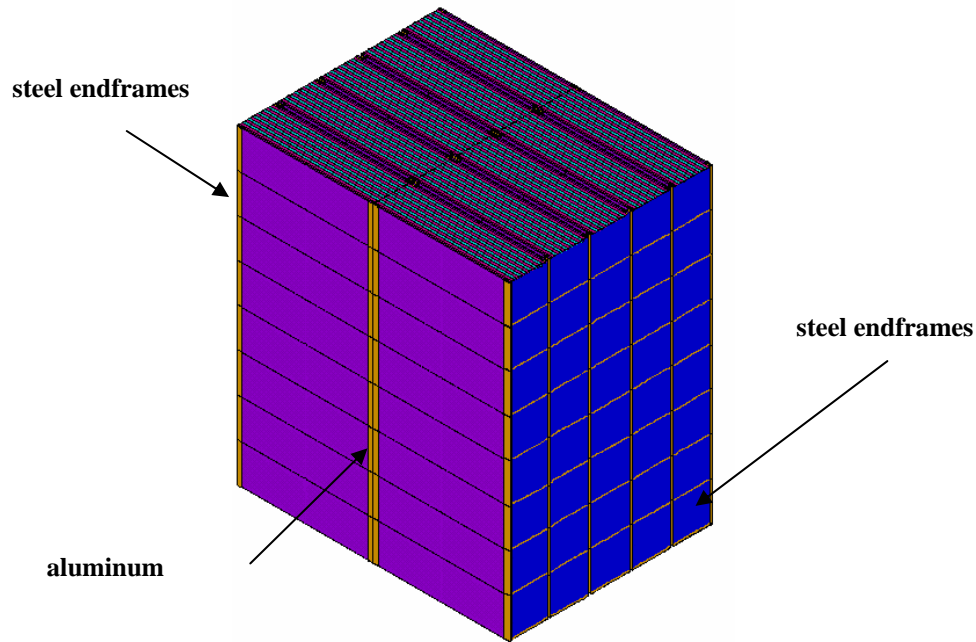


Figure 1. A Five-deep stack of RPC modules. The complete detector is 75 modules deep.

Implementation in GEANT

The detector described above has been accurately implemented in GEANT. The gaps between modules, the gaps between RPCs and the dead spaces due to plastic spacers along the outer edge of the RPC chambers have all been included in the geometrical description of the detector. Spacers internal to the RPC chambers have not been included in the geometrical description of the detector. The inefficiency that results from the internal spacers is included in an overall 5% random inefficiency for each RPC chamber. The GEANT implementation of the detector geometry is shown in Figures 4 and 5.

Wood is not one of the default materials available in GEANT. However, GEANT allows one to construct complex materials from simple ones. The particleboard absorber has been modeled in GEANT using a mixture of carbon, oxygen and hydrogen (49%, 45% and 6%, respectively) with a density of 0.70 g/cc. GEANT calculates a radiation length of 55.5 cm for this mixture. Mixtures for the RPC glass and gas are also constructed from their component parts.

Event Generation

Neutrino interactions are generated throughout the entire volume of the detector, including the volume outside the fiducial cut. The vertex location is weighted by the

number of target nuclei in the various materials that make up the detector. Once the vertex is selected, the NEUGEN3 event generator is called. $\nu_\mu \rightarrow \nu_e$ signal events, ν_μ Charged Current (CC) events, ν_μ Neutral Current (NC) events and beam ν_e events are generated separately. The signal events are generated with a flat neutrino energy spectrum from 0.1 to 3.0 GeV and the background events are all generated with a flat distribution between 0.1 and 20 GeV.

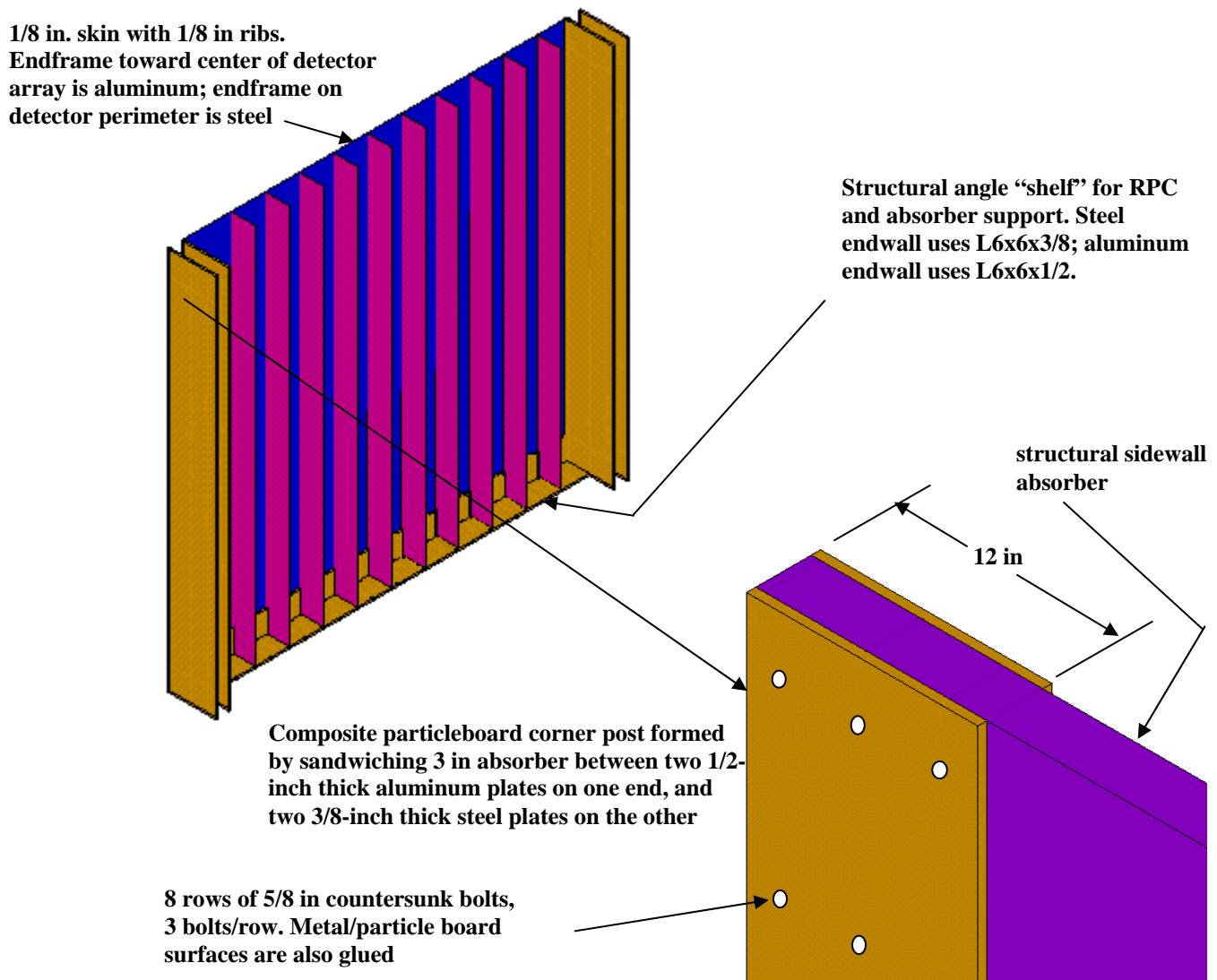


Figure 2. Endframe Assembly

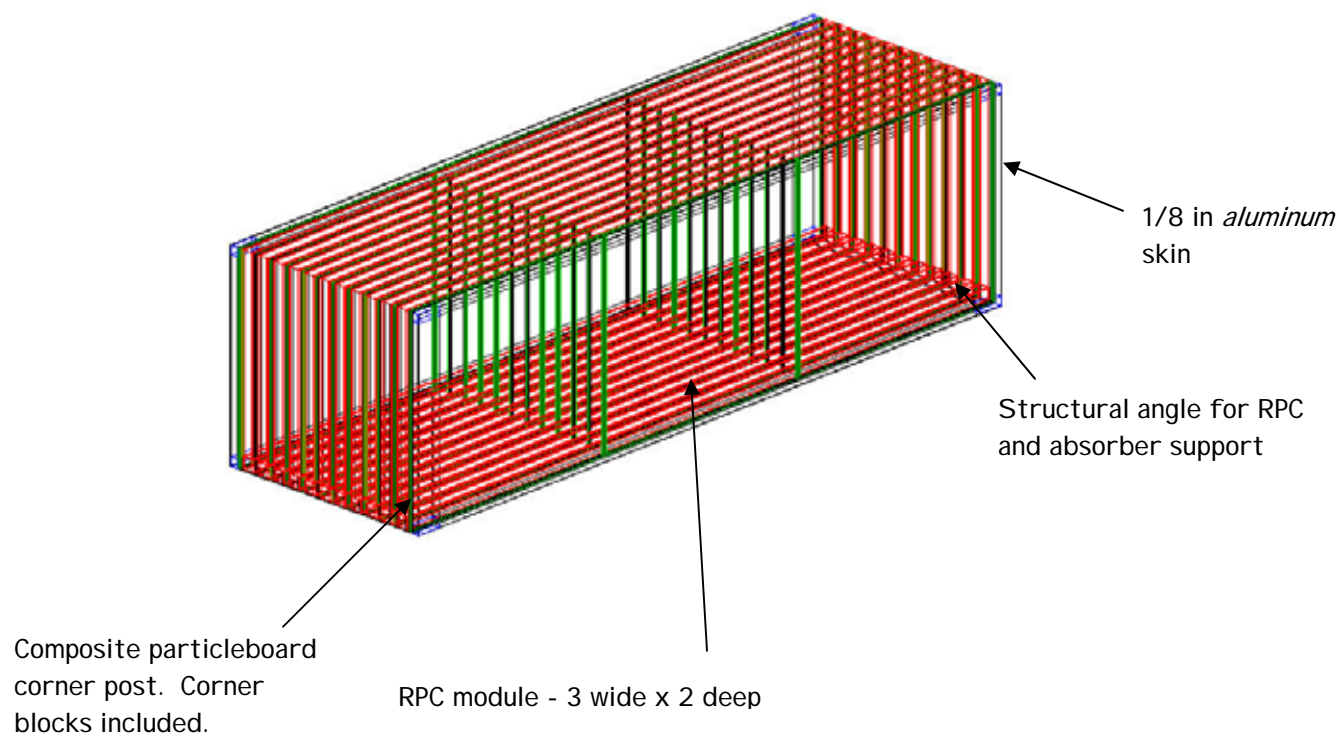


Figure 3. GEANT implementation of an RPC module.

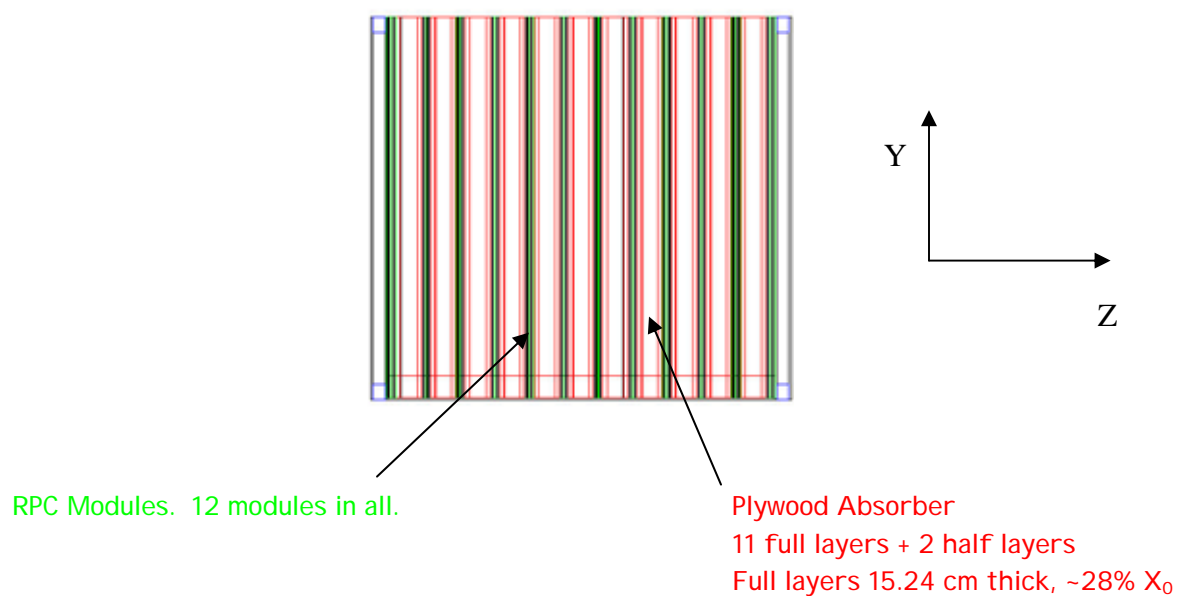


Figure 4. GEANT implementation of an RPC module, side view.

The particles generated by NEUGEN3 and all of the daughter particles generated by their interactions are input to GEANT and tracked through the detector. 10 keV cutoffs are used for the various physics processes. 95% of the particles that experience energy loss in the gas volume of an RPC produce a hit. The 5% loss is a built-in random inefficiency. The plastic spacers around the edge of the chambers results in additional inefficiency that is accounted for in the geometrical description of the detector. When energy loss in the gas volume occurs, the track is extrapolated to the readout strips on each side of the RPC detector unit and a hit is recorded on the appropriate X and Y strips. Whenever a hit is recorded there is a finite probability of inductive cross talk or charge sharing. This effect has been measured on prototype chambers at Fermilab as a function of the distance from the extrapolated track to the adjacent strip [3]. The results of those measurements have been fit and the fit is used to parameterize the probability of cross talk in the Monte Carlo. The measured data points and the fit to them are shown in Figure 5a. The cross-talk measurements were made using single-gap RPC chambers while the simulated detector contains back-to-back RPCs sandwiched between a pair of readout boards, as shown in Figure 6. The cross talk has never been measured for this configuration. To the extent that inductive cross talk is a solid angle effect, the cross talk on a particular readout board will be different for the near and the far RPC. In the simulation, the parameterization in Figure 5a is used to test for cross talk on the nearest readout board to a given RPC and the parameterization in Figure 5b is used for the further of the two readout boards. Figure 5b uses the same data points as Figure 5a, but a given cross-talk probability occurs twice as far from the neighboring strip as before. For example, in Figure 5a the probability of cross talk on the neighboring strip when the extrapolated track is 0.25 cm from the boundary between the two strips is 0.389. In Figure 5b a cross-talk probability of 0.389 occurs at a distance of 0.50 cm from the boundary.

Approximately 1,000,000 events are generated for each of the 4 data sets ($\nu_\mu \rightarrow \nu_e$ signal events, ν_μ CC, ν_μ NC and beam ν_e). The hit information along with information from NEUGEN regarding the initial neutrino interaction is written out to an unformatted text file for each event. The data files are saved for subsequent analysis.

Event Reconstruction

The output data files from GEANT are read into a reconstruction program. The X-Z and Y-Z views are generally treated independently. A Hough transform is performed on the hits in each view to find the most likely set of hits that approximate a straight line. The Hough transform steps through slope-intercept space to find the maximum number of hits that lie within a preset minimum distance of a given trajectory. The procedure is repeated with finer binning in slope-intercept space to find the best track parameters in each view. In order to find additional tracks, the Hough transform procedure is repeated on the hits that have yet to be associated with a previously identified track. An electron candidate is identified by the pair of tracks, 1 from each view, with the highest Hough probability that begin within ± 1 detector planes of one another. The hits that define the final track candidate in each view are fit to a parabolic trajectory to allow for the considerable

multiple scattering inherent in the detector design. Ntuples are produced by the reconstruction program and are used for the final analysis.

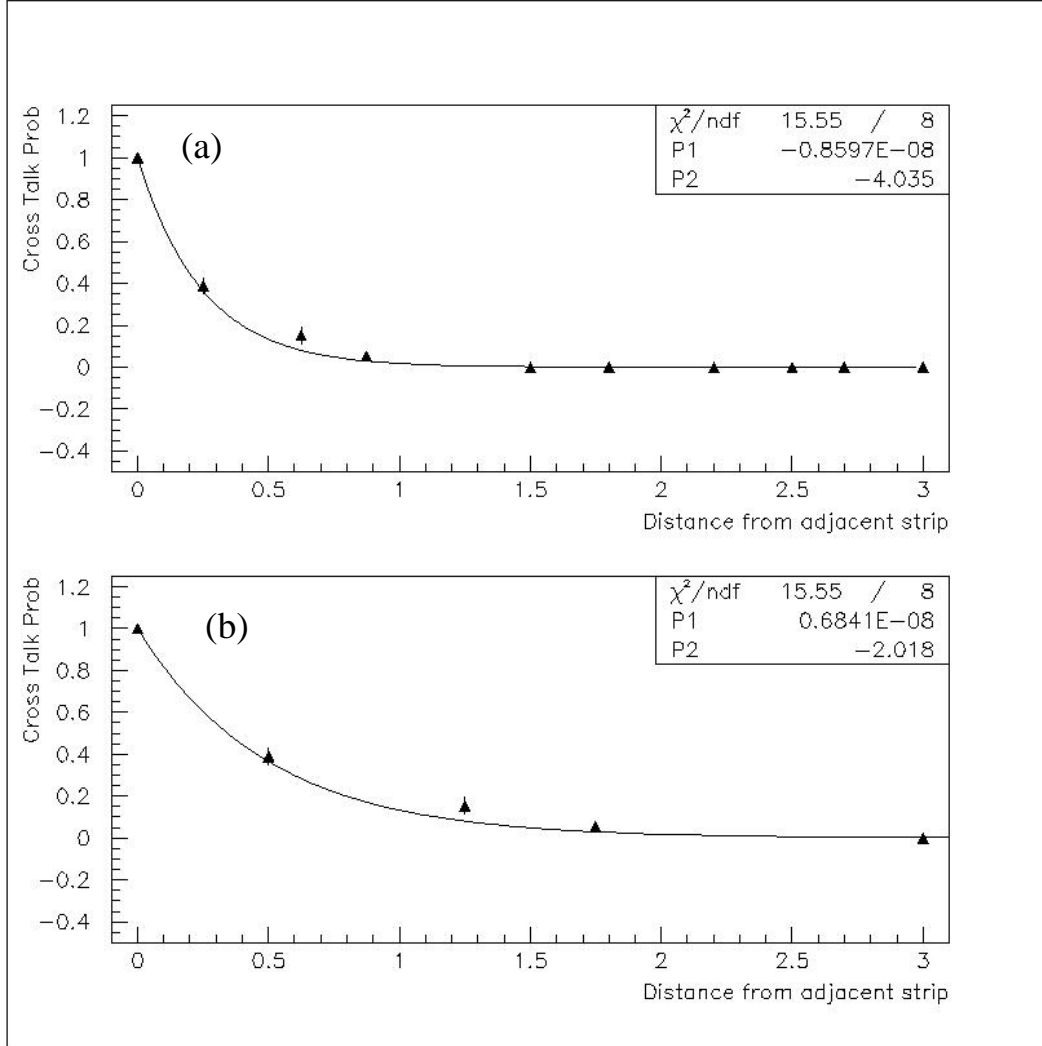


Figure 5. Inductive cross-talk (charge sharing) probability for back-to-back RPCs sandwiched between a single pair of readout boards. a) For the nearest of the two readout boards, the probability of cross-talk on an adjacent strip as a function of the distance between the extrapolated track and the adjacent strip; b) For the farthest of the two readout boards, the probability of cross-talk on an adjacent strip as a function of the distance between the extrapolated track and the adjacent strip.

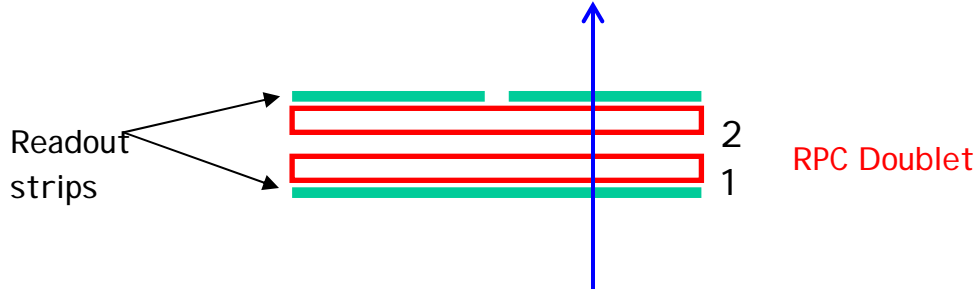


Figure 6. Back-to-back RPC chambers sandwiched between a single pair of readout boards.

Event Weighting

The signal events are generated with a flat neutrino energy spectrum from 0.1 to 3.0 GeV and the background events are generated with a flat distribution between 0.1 and 20 GeV. In order to represent the event distributions expected at the far detector the events have to be appropriately weighted for an off axis detector 810 km from Fermilab, 10 km off-axis. The NUMI medium energy beam configuration is assumed. The ν_μ survival probability is calculated with $\text{Sin}^2 2\theta_{23} = 1.0$, $\Delta m_{32}^2 = 2.5 \times 10^{-3} (\text{eV}/c)^2$. The oscillation probability for $\nu_\mu \rightarrow \nu_e$ is calculated using $\text{Sin}^2 2\theta_{13} = 0.1$. The rate of ν_μ NC events is scaled from CC events using the NC/CC ratio as a function of neutrino energy. NC interactions from ν_μ that oscillate to ν_τ also contribute to the background since they cannot be distinguished from ν_μ NC interactions in the detector. The overall normalization is based on a 50 kton detector and 3.7×10^{20} protons on target per year for 5 years. The number of events expected at the far detector is shown in Table 1. The final oscillated beam spectra are shown in Figure 7.

	$\nu_\mu \rightarrow \nu_e$	ν_μ NC	ν_μ CC	Beam ν_e
Events Before Oscillation		10650	31500	870
Events after Oscillation	615	10650	14225	870

Table 1. Expected number of raw events for the signal and backgrounds before reconstruction and analysis at a far detector 810 km from Fermilab, 10 km off-axis. The numbers are for a 50 kt detector running for 5 years with 3.7×10^{20} p/yr.

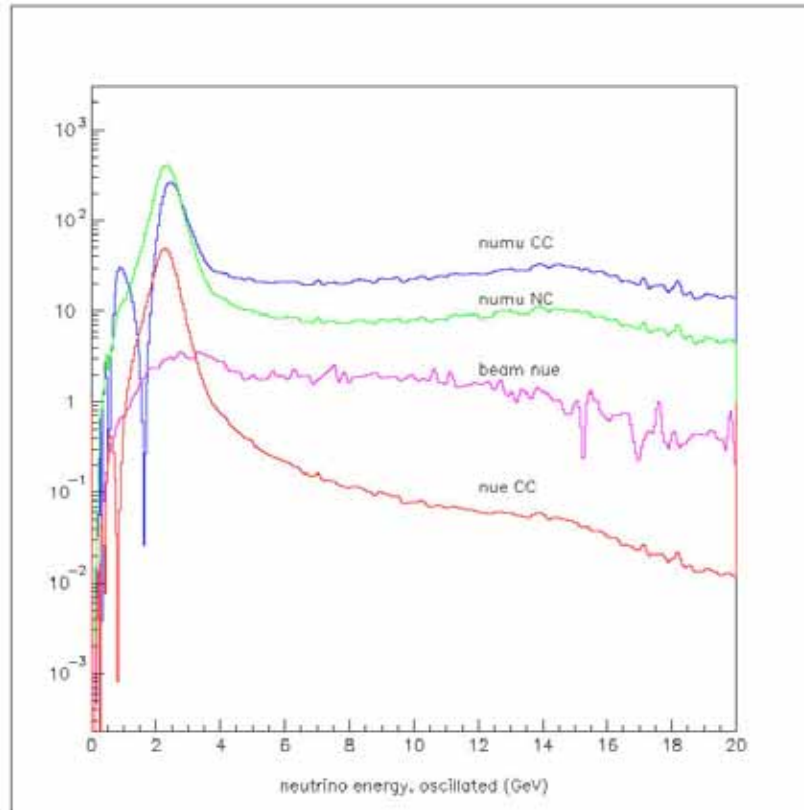


Figure 7. Neutrino energy spectra at the far detector, 810 km from Fermilab, 10 km off axis

Event Selection

The event selection proceeded in two stages. In the first stage a set of cuts were applied to distributions where the signal and background were relatively distinct. The distributions that are cut on are:

- Number of hits outside the fiducial volume
- Total number of hits in the event
- Length of the electron candidate track in each view
- The number of hits on the candidate electron track in each view
- The fraction of the total hits in the event on the electron candidate track

Plots of these distributions for the signal and background processes are shown in Figures 8-11.

The second stage of the analysis consists of forming one-dimensional maximum likelihood ratios for the signal and each of the backgrounds. The distributions are normalized to 1.0 and define the probability that a particular event came from that distribution. The total likelihood for signal and each of the backgrounds results from multiplying all of the probabilities together. Three log likelihood ratios are formed between the signal hypothesis and the three background hypothesis. These log likelihood ratios are cut on to arrive at the final event sample. The distributions that are used to form the likelihood probabilities are:

- Track width distribution in the X-Z and Y-Z views
- Number of planes with hits that contribute to the electron track candidate
- Average number of hits per plane that contribute to the electron track candidate
- Cosine of the angle between the neutrino beam direction and the electron track candidate
- The largest gap in the electron track candidate
- The fraction of the total hits in the event on the electron candidate track.

Plots of these distributions for the signal and background processes are shown in Figures 12-17 and the final likelihood ratios are shown in Figures 18-20. The cuts on all of these values are listed in Table 2.

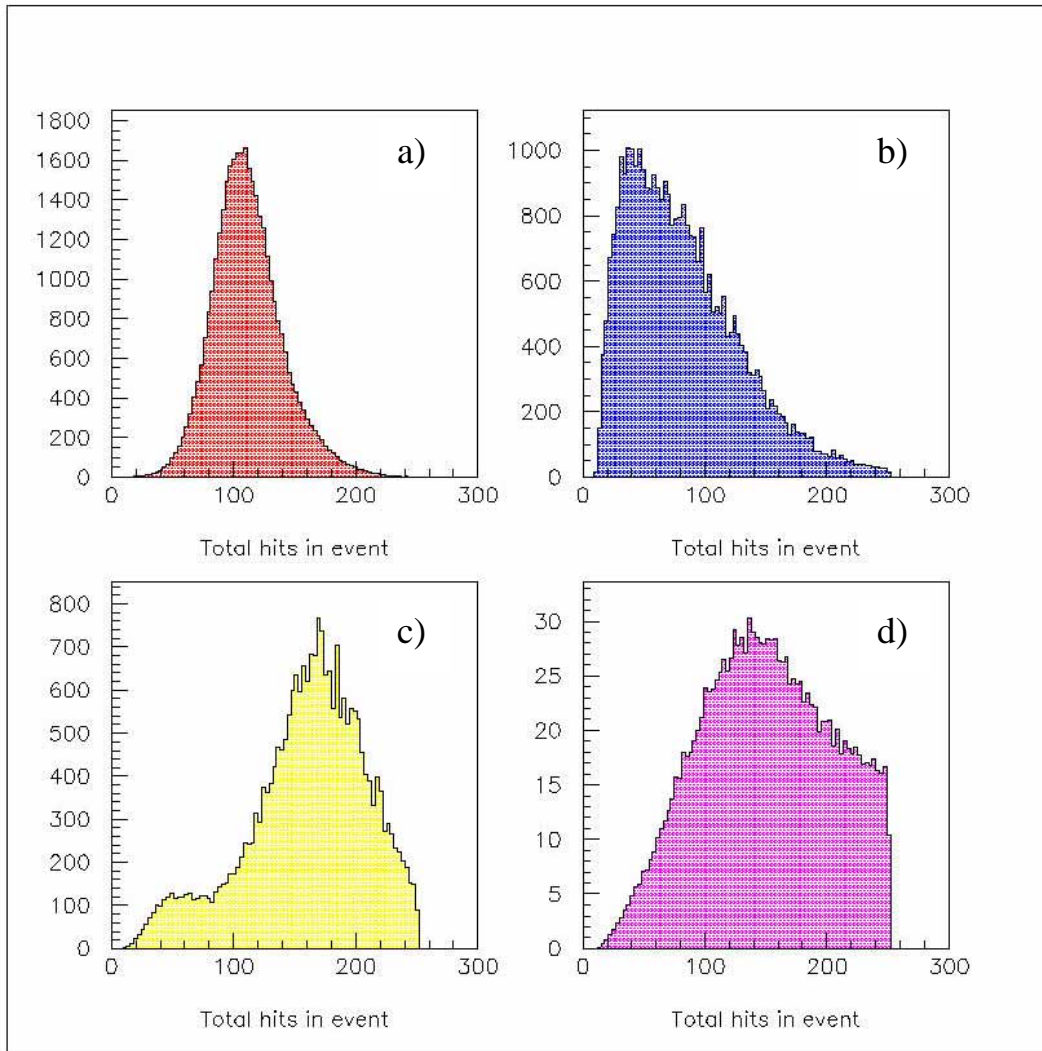


Figure 8. Distribution of total number of hit strips in event for a) $\nu_\mu \rightarrow \nu_e$, b) ν_μ NC, c) ν_μ CC and d) Beam ν_e . Events with more than 250 hits are not processed in order to speed up the reconstruction program explaining the hard cut-off in the beam ν_e distribution.

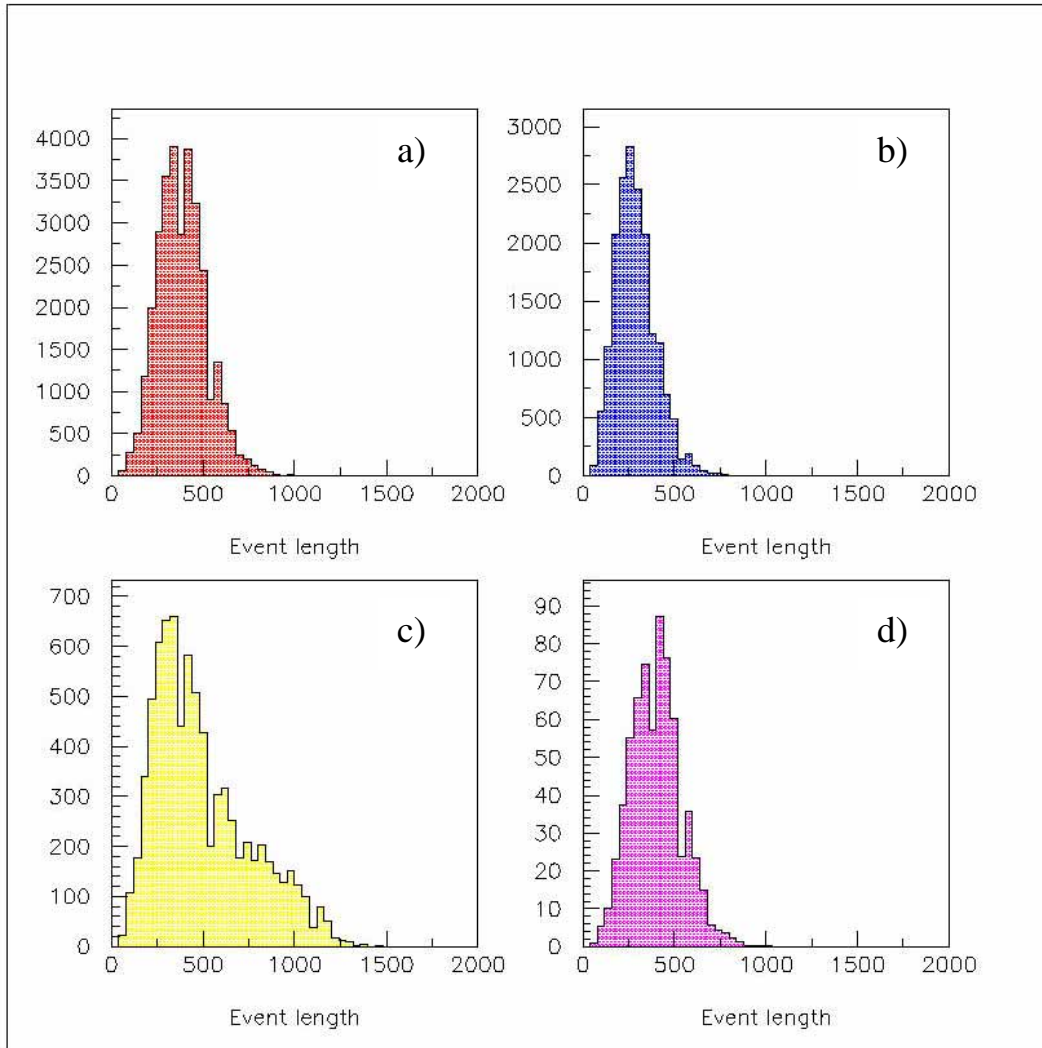


Figure 9. Track length distribution in the X-Z view for a) $\nu_\mu \rightarrow \nu_e$, b) ν_μ NC, c) ν_μ CC and d) Beam ν_e . The distributions in the Y-Z view are nearly identical. The units on the horizontal axis are cm.

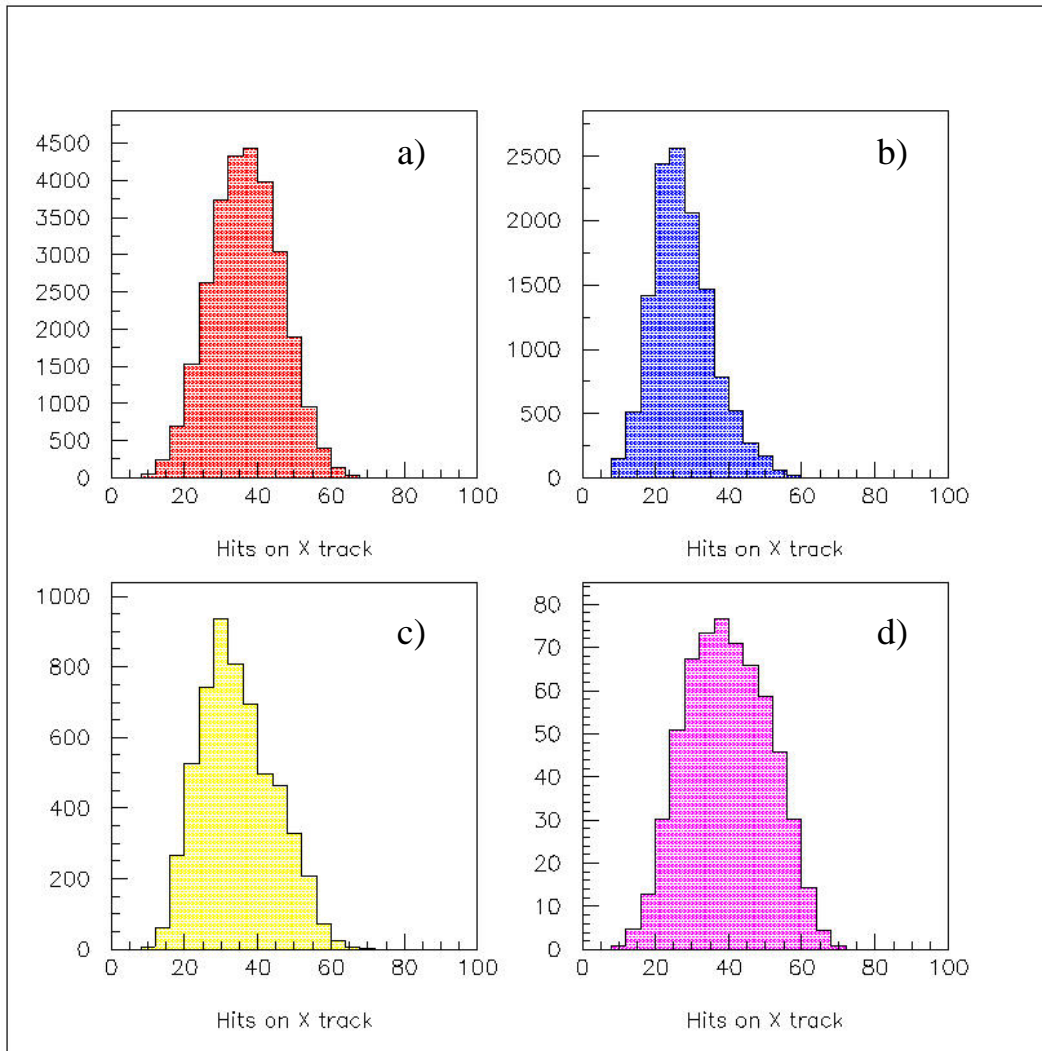


Figure 10. Distribution of the number of hit strips on the electron track candidate in the X-Z view for a) $\nu_\mu \rightarrow \nu_e$, b) ν_μ NC, c) ν_μ CC and d) Beam ν_e . The distributions in the Y-Z view are nearly identical.

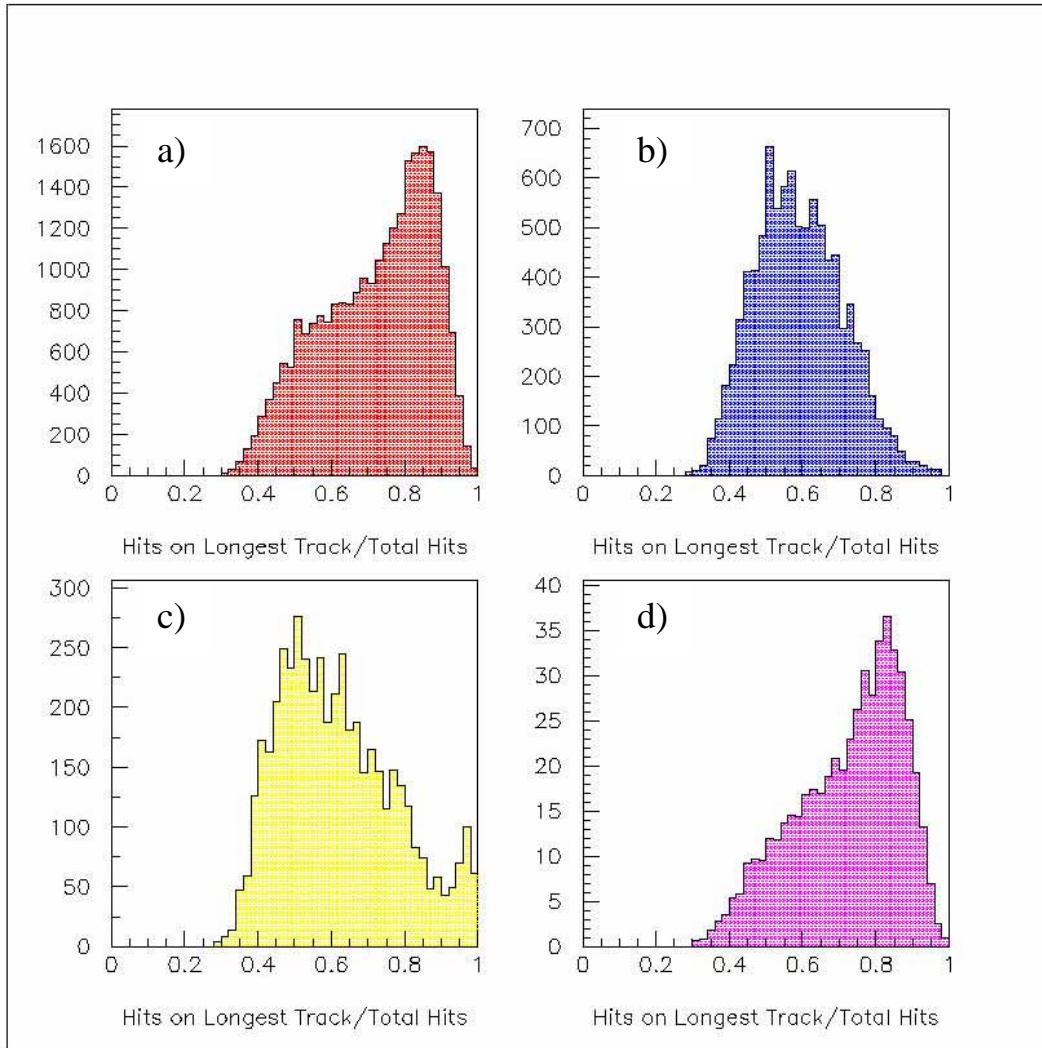


Figure 11. Distribution of $1-y$ for a) $\nu_\mu \rightarrow \nu_e$, b) ν_μ NC, c) ν_μ CC and d) Beam ν_e . $1-y$ is constructed from the total number of hit strips on the candidate electron track divided by the total number of hit strips in the event.

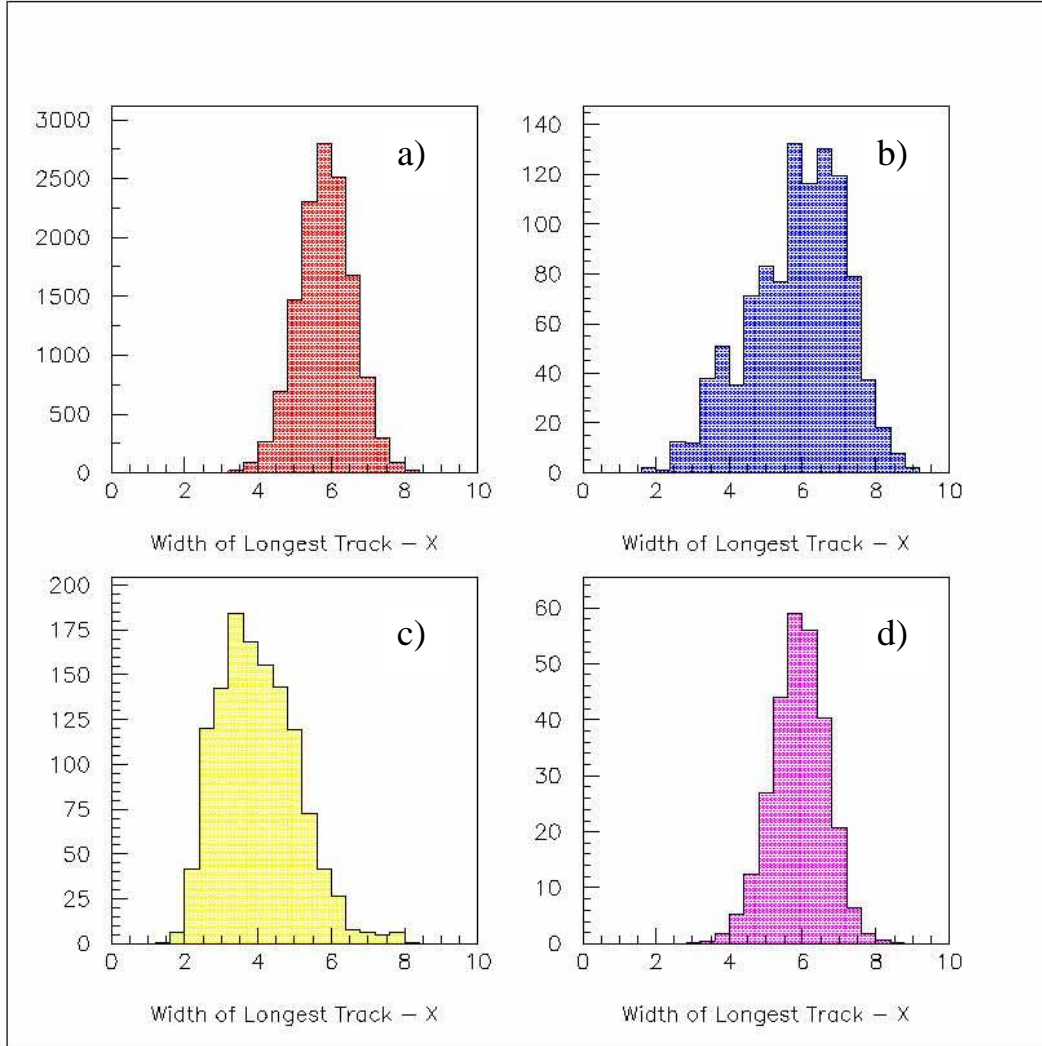


Figure 12. Track width distributions in the X-Z view for a) $\nu_\mu \rightarrow \nu_e$, b) ν_μ NC, c) ν_μ CC and d) Beam ν_e . The track width is defined as $\sum (x_{\text{pred}} - x_{\text{hit}})^2$ where x_{pred} is the x position predicted from the fitted track trajectory. The sum runs over all hits within 15 cm of the fitted track trajectory. The distributions in the Y-Z view are nearly identical.

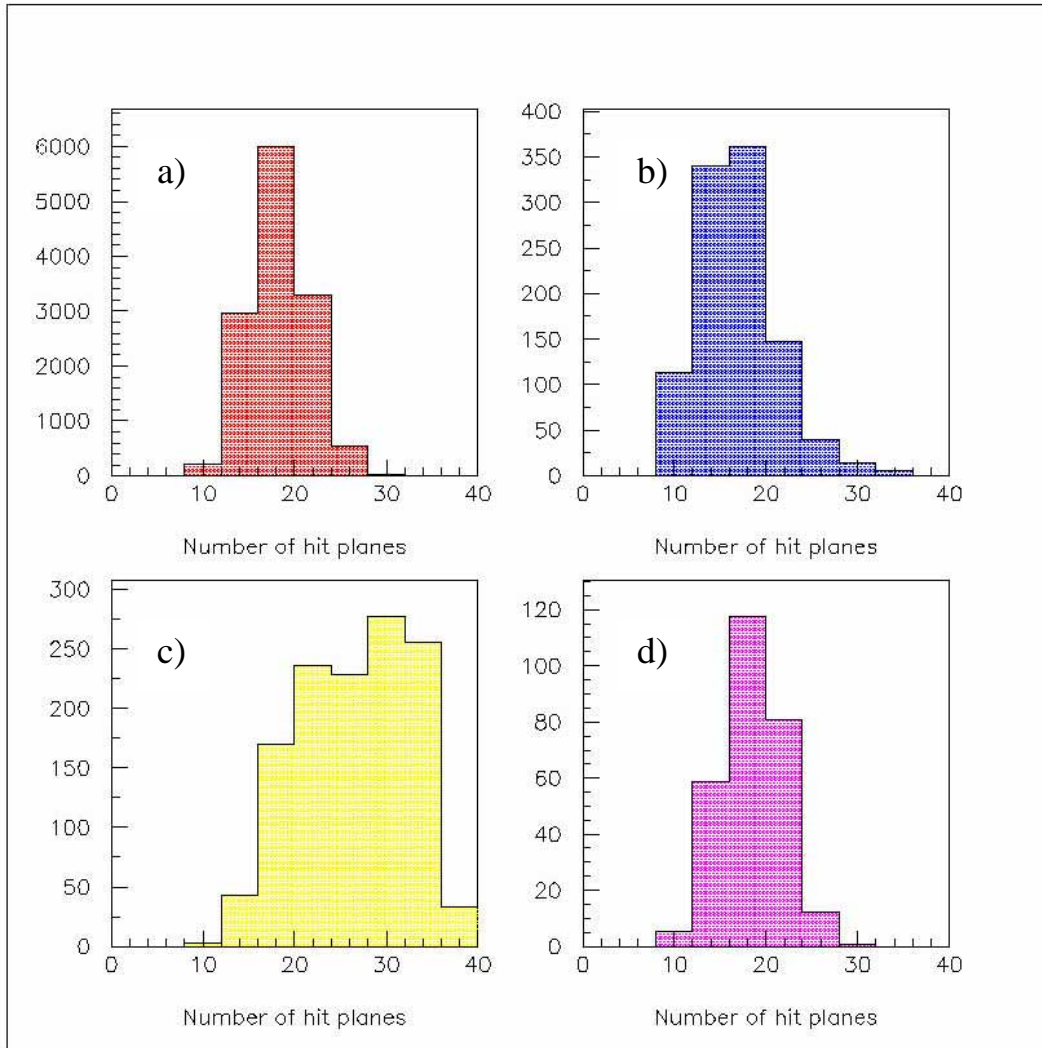


Figure 13. The distribution of the number of planes with hits that contribute to the electron track candidate for a) $\nu_\mu \rightarrow \nu_e$, b) ν_μ NC, c) ν_μ CC and d) Beam ν_e .

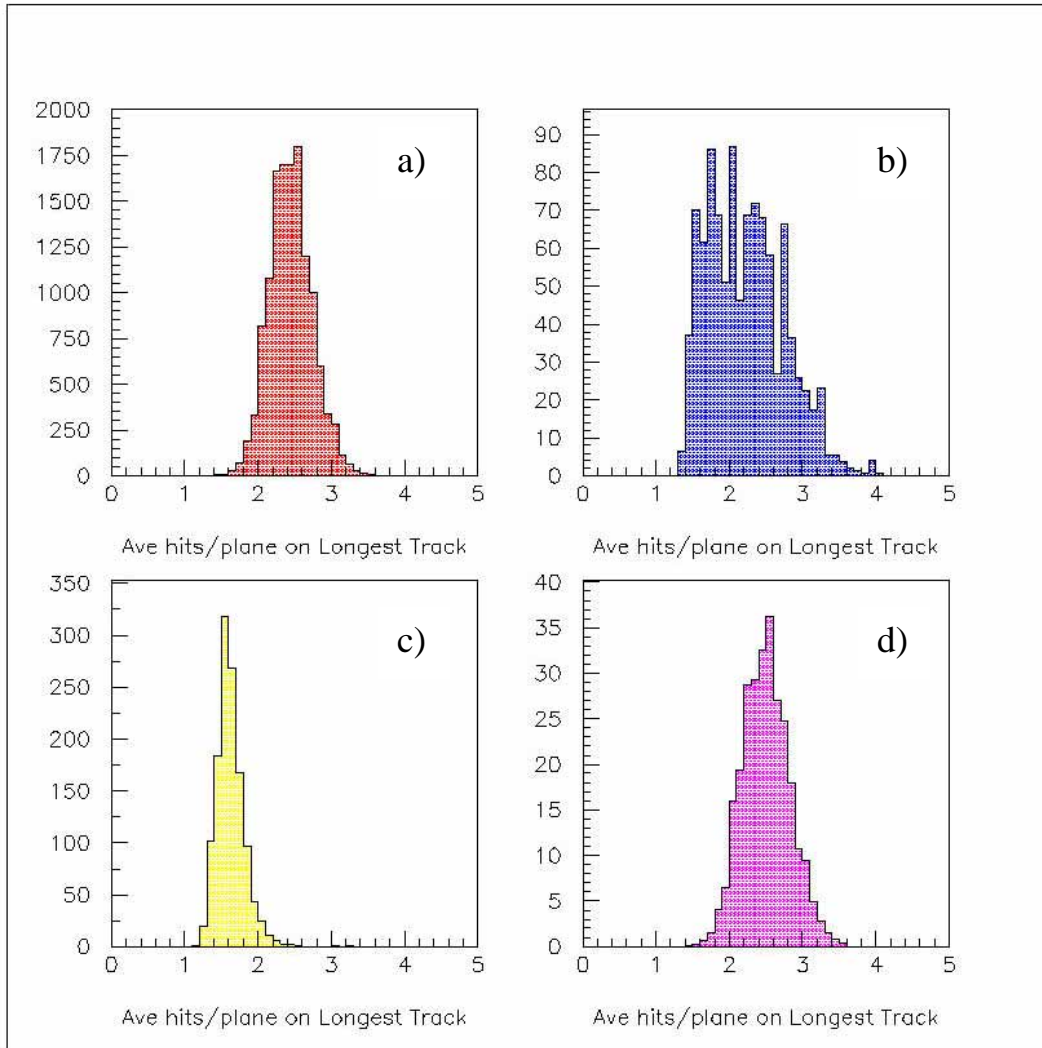


Figure 14. Distribution of the average number of hits per plane on the trajectory of the electron track candidate for a) $\nu_\mu \rightarrow \nu_e$, b) ν_μ NC, c) ν_μ CC and d) Beam ν_e .

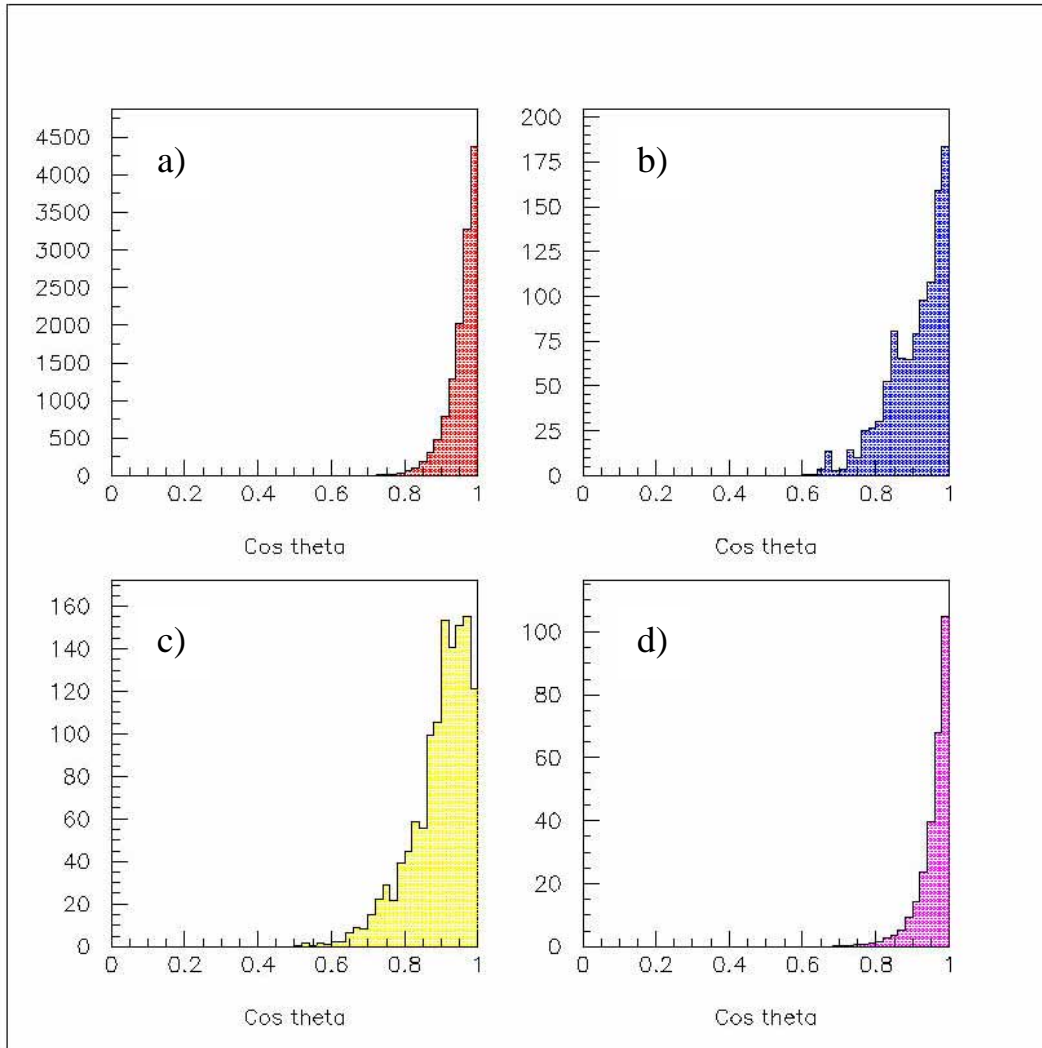


Figure 15. Distribution of $\text{Cos } \theta$ for a) $\nu_\mu \rightarrow \nu_e$, b) ν_μ NC, c) ν_μ CC and d) Beam ν_e . θ is the angle between the beam and the candidate electron track.

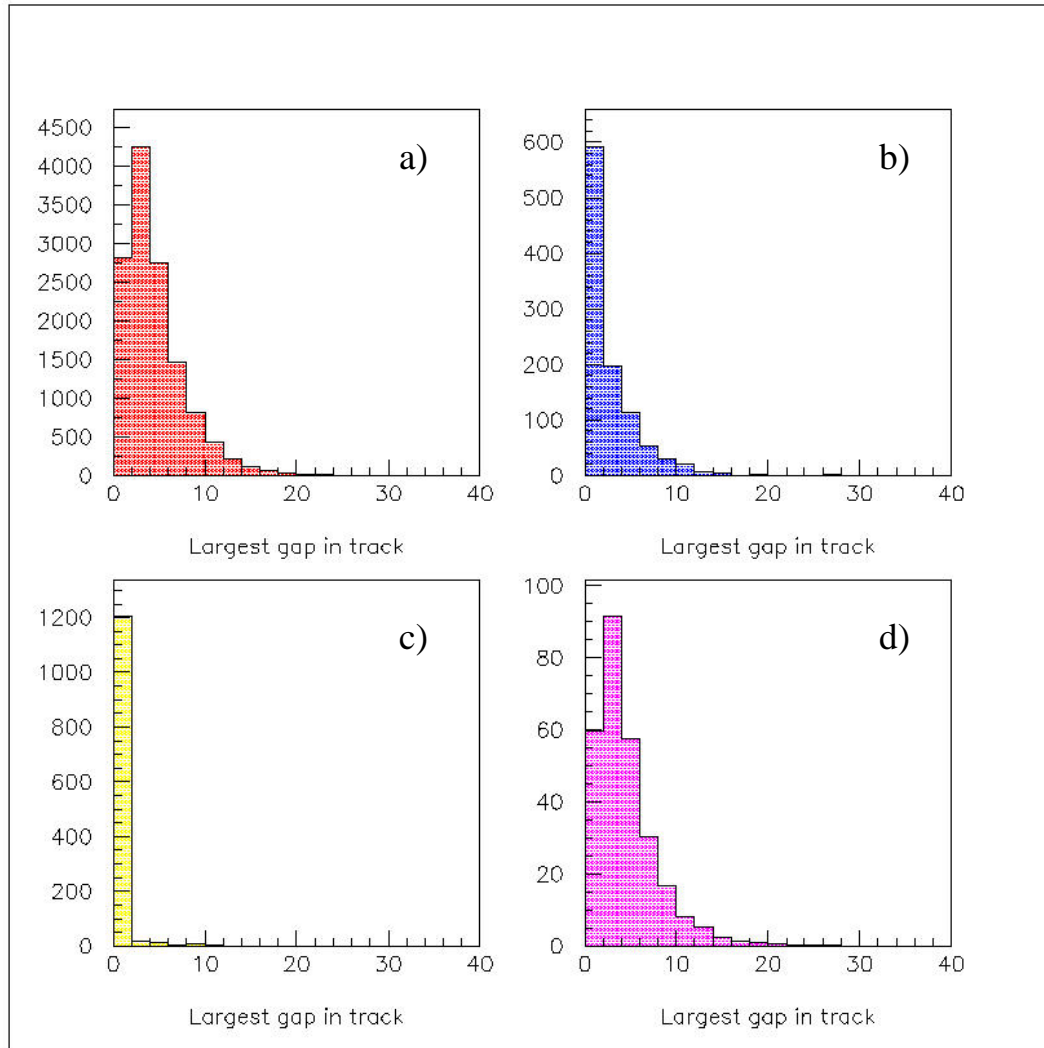


Figure 16. Distribution of the largest gap in the candidate electron track for a) $\nu_\mu \rightarrow \nu_e$, b) ν_μ NC, c) ν_μ CC and d) Beam ν_e .

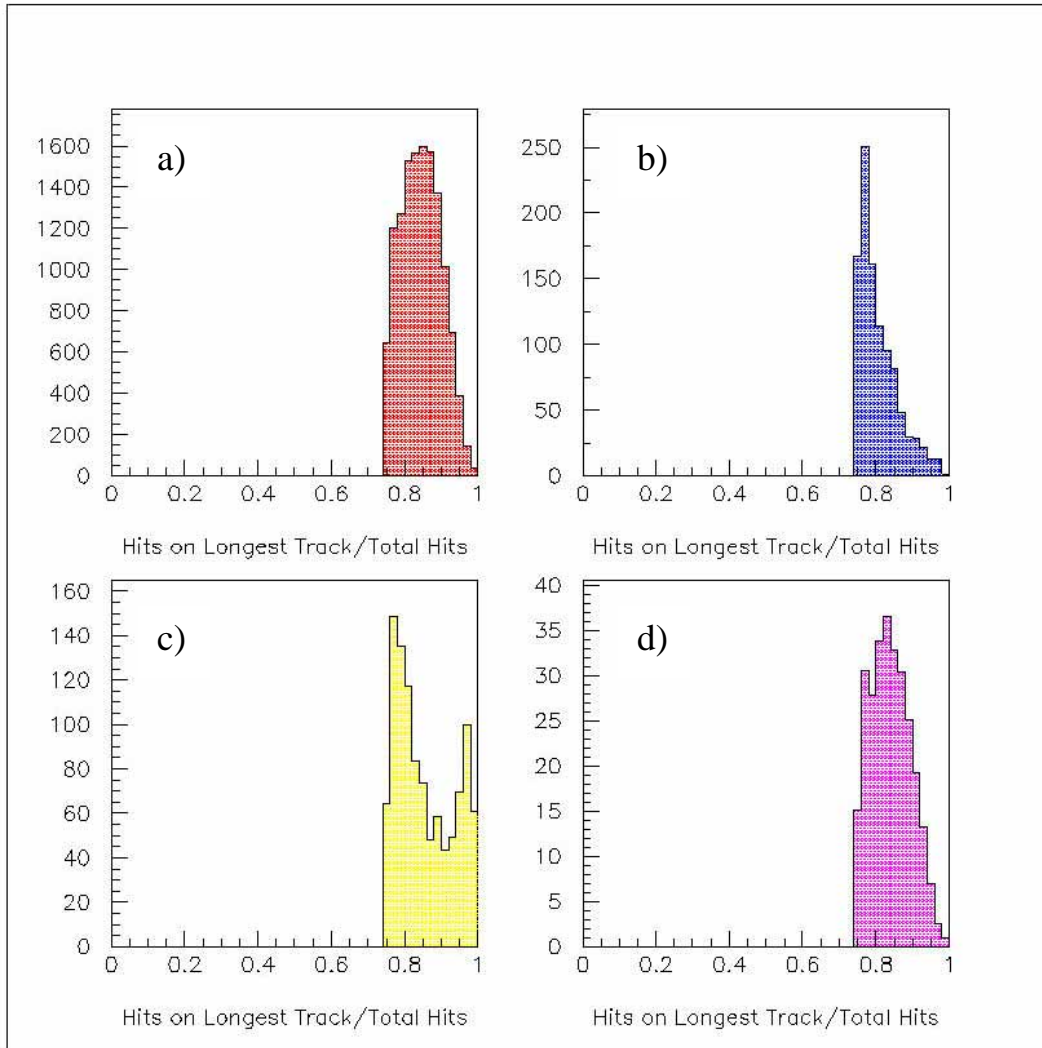


Figure 17. Distribution of $1-y$ for a) $\nu_\mu \rightarrow \nu_e$, b) ν_μ NC, c) ν_μ CC and d) Beam ν_e . $1-y$ is constructed from the total number of hit strips on the candidate electron track divided by the total number of hit strips in the event. A cut at 0.75 is made on these distributions early in the analysis. The resulting distributions shown here are used in the likelihood analysis.

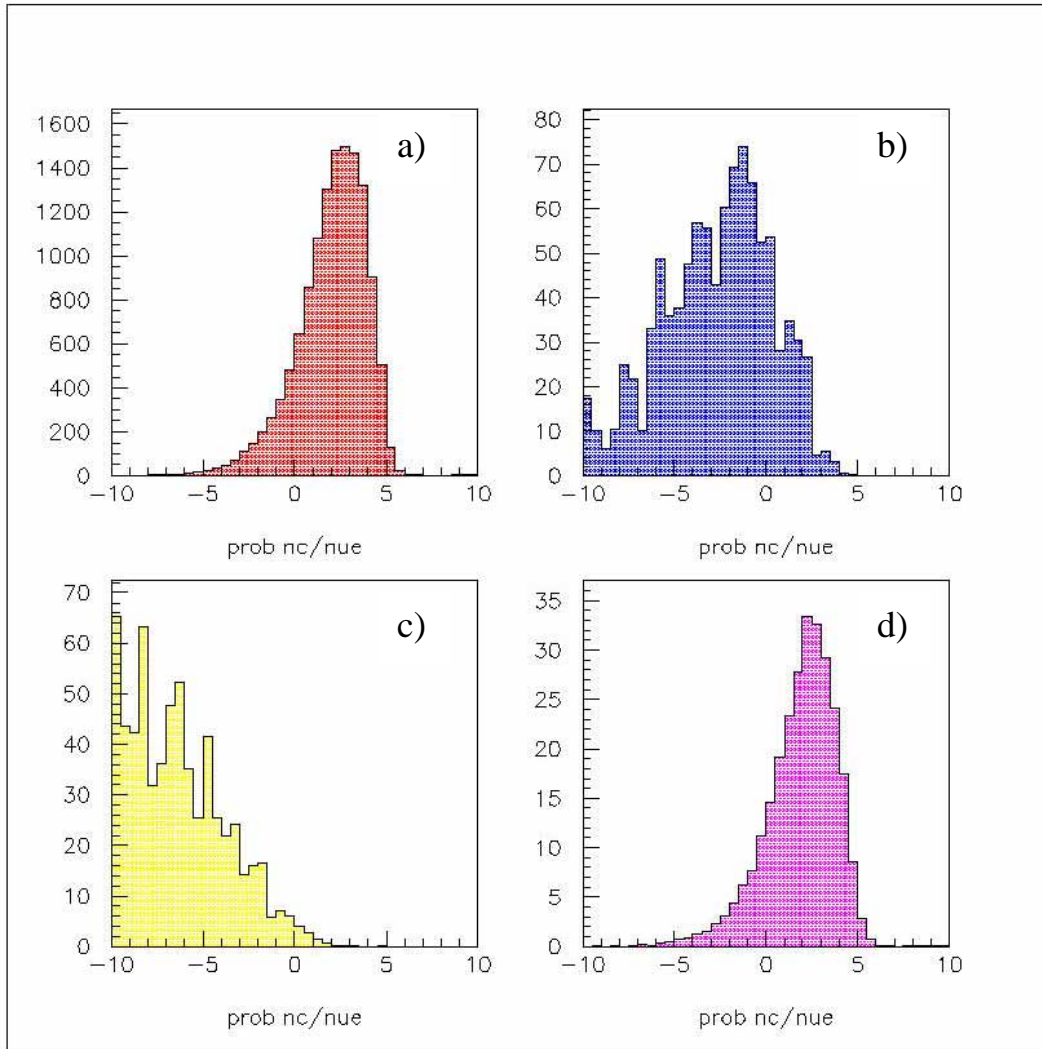


Figure 18. The log likelihood ratio of the ν_μ NC hypothesis to the $\nu_\mu \rightarrow \nu_e$ hypothesis for a) $\nu_\mu \rightarrow \nu_e$, b) ν_μ NC, c) ν_μ CC and d) Beam ν_e .

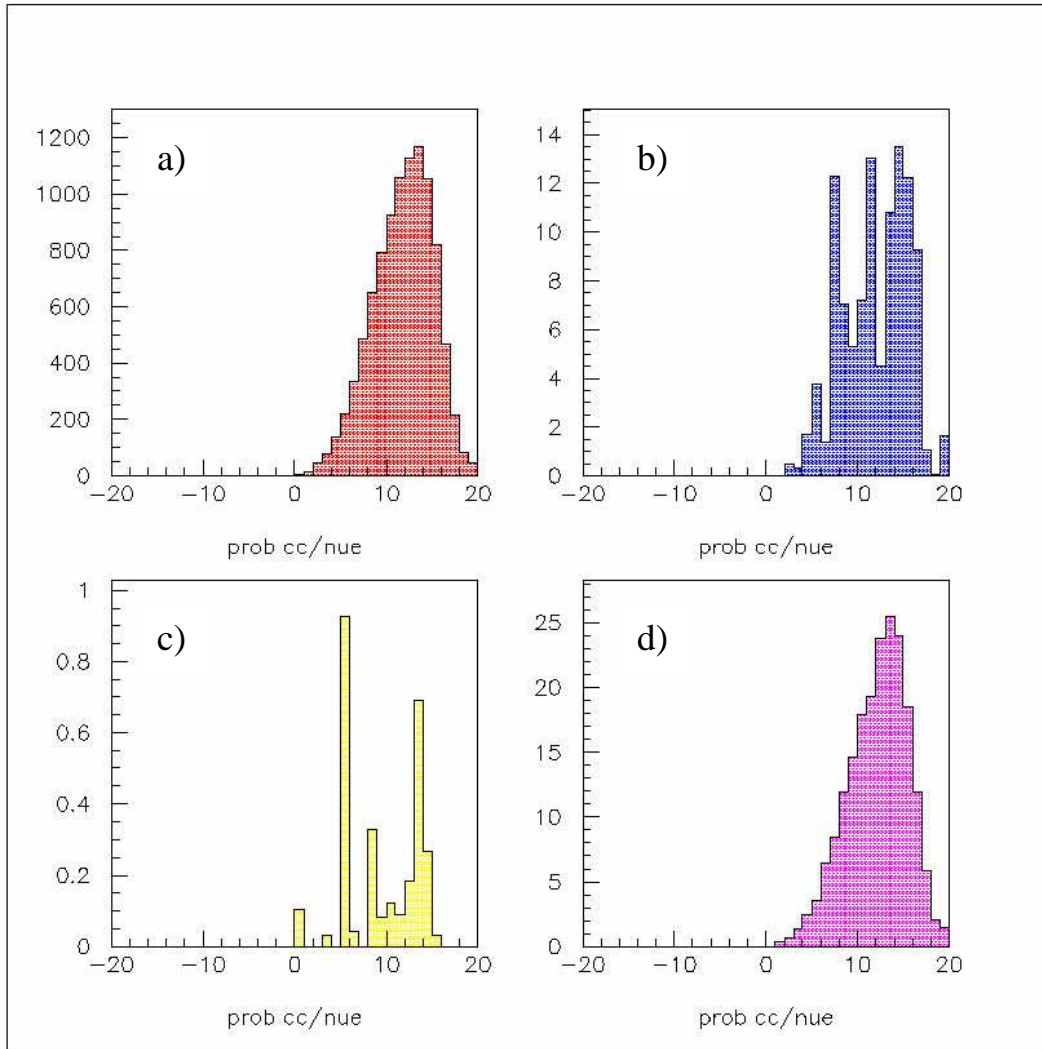


Figure 19. The log likelihood ratio of the ν_μ CC hypothesis to the $\nu_\mu \rightarrow \nu_e$ hypothesis for a) $\nu_\mu \rightarrow \nu_e$, b) ν_μ NC, c) ν_μ CC and d) Beam ν_e .

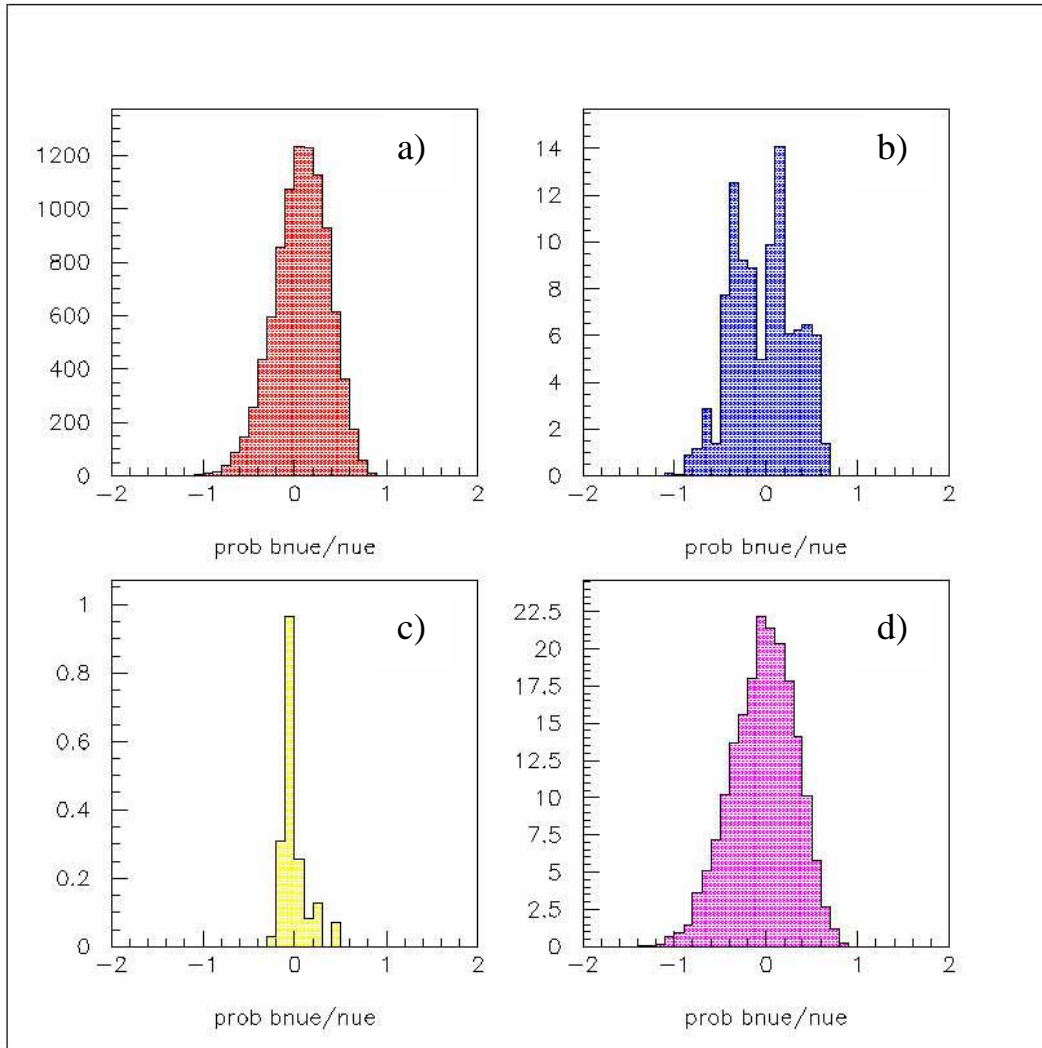


Figure 20. The log likelihood ratio of the Beam ν_e hypothesis to the $\nu_\mu \rightarrow \nu_e$ hypothesis for a) $\nu_\mu \rightarrow \nu_e$, b) ν_μ NC, c) ν_μ CC and d) Beam ν_e .

Distribution	Cut
Number of hits outside fiducial volume	<3
Total number of hit strips	60 to 150
Length of electron candidate	200 to 800 cm
Number of hits on electron track	20 to 60
Hits on electron track/total hits in event	>0.75
NC log likelihood ratio	>1.0
CC log likelihood ratio	>6.0
Beam ν_e log likelihood ratio	>-0.4

Table 2. Cuts on the various distributions for the nominal RPC analysis.

Results

The results for the nominal RPC detector are listed in Table 3. The first row of the table lists the numbers of weighted events generated for each mode and the 7 subsequent rows show the number of weighted events that pass the cuts. The row showing the number of events surviving after implementation of the likelihood cuts includes cuts on all 3 log likelihood ratios. The number of events that survive the likelihood analysis divided by the number of generated events defines the efficiency. The efficiency is then multiplied by the expected number of events from Table 1 to arrive at the actual number of observed events. A Figure-of-Merit (FOM) can be defined as

$$\text{FOM} = \text{signal}/\sqrt{\text{background}} = 123/\sqrt{12.7+1.1+11.5} = 24.5.$$

This can be used to make general comparisons with different detector configurations and other detector technologies.

	$\nu_\mu \rightarrow \nu_e$	ν_μ NC	ν_μ NC	Beam ν_e
Generated	53540	95013	124944	4181
Reconstructed	49213	46135	72467	2186
Fiducial cut	35321	34011	17020	1311
Total Hits	31007	17615	9908	991
Track length	25797	11322	5506	526
Hits on track	12470	1218	439	225
1-y	12038	848	224	214
Likelihood	7578	114	10.0	78
Efficiency	0.14	0.001	8.0×10^{-5}	0.02
Observed Events	123	12.7	1.1	11.5

Table 3. Results for the nominal RPC detector. The first row of the table lists the numbers of events generated for each mode after weighting by the relevant beam spectrum. The 7 subsequent rows show the number of weighted events that pass the cuts. The last row is the number of observed events based on the calculated efficiencies in the table and the number of raw events from Table 1.

References

- [1] I. Ambats et al. “Proposal to Build an Off-Axis detector to Study $\nu_\mu \rightarrow \nu_e$ Oscillations in the NuMI Beamline”, P929 Proposal;
- [2] B. Wands, “An Aluminum/Steel Endframe design for an Off-Axis detector Module”, Off-Axis-NOTE-0018.
- [3] V. Makeev, private communication.

